International Journal of Solids and Structures 96 (2016) 145–152

Contents lists available at ScienceDirect

International Journal of Solids and Structures

journal homepage: www.elsevier.com/locate/ijsolstr

A hyperboloid structure as a mechanical model of the carbon bond

I.E. Berinskii [a,b,*], A.M. Krivtsov [b,c]

[a] School of Mechanical Engineering, Tel Aviv Univeristy, Ramat Aviv, Tel Aviv 69978, Israel
[b] Peter the Great St. Petersburg Polytechnic University, 29, Politechnicheskaya str., St. Petersburg, 195251, Russia
[c] Institute for Problems in Mechanical Engineering RAS, 61, Bolshoy pr. V. O., St. Petersburg, 199178, Russia

ARTICLE INFO

Article history:
Received 16 September 2015
Revised 3 May 2016
Available online 18 June 2016

Keywords:
Mechanics of carbon bond
Mechanics of nanostuctures
Hyperboloid model
Structural model
Molecular mechanics

ABSTRACT

We present a new mechanical model of interatomic bonds, which can be used to describe the elastic properties of the carbon allotropes, such as graphite, diamond, fullerene, and carbon nanotubes. The interatomic bond is modeled by a hyperboloid–shape truss structure. The elastic characteristics of this bond are determined. Previous known structural models also used elastic elements (beams, trusses) to simulate a carbon bond. However unlike them our model satisfies to the correct ratio of the longitudinal and lateral stiffness, observed from the previous experimental and theoretical results. Parameters of the bond in application for graphene and diamond were determined.

1. Introduction

Mechanical properties of carbon nanostructures have been extensively studied by scientists all over the world since the middle of the twentieth century. The elastic properties of two most common allotropes of carbon: diamond and graphite were experimentally determined in works McSkimin and Andreatch Jr (1972); McSkimin and Bond (1957) and Blakslee et al. (1970), respectively. Due to the unique crystal structure, diamond and lonsdaleite are considered as the most durable of the existing materials. At the same time it was predicted that graphite should also have an outstanding tensile strength in the basal plane, but the plane orthogonal to the base has significantly lower tensile strength (Blakslee et al., 1970; Bosak et al., 2007). Discovery of such materials as fullerenes (Kroto et al., 1985), carbon nanotubes (Iijima et al., 1991), and graphene (Geim and Novoselov, 2007) at the turn of the present century, warmed up the interest of the scientific community to the properties of carbon and the structures it is capable to form.

A key point in the study of the carbon allotropes and its properties at the micro level is the choice of a model describing the interatomic bonds. The ab initio methods developed in the past decade due to the advances of quantum physics and chemistry are widely used to model carbon nanostructures (Bichoutskaia et al., 2006; Kudin et al., 2001; Yanovsky et al., 2009; Zhou et al., 2001). Apparently, they are the most precise and predictively valid methods, but due to the high complexity and high computational costs, they are rarely used to describe even relatively small nanostructures, not to mention the objects of the size of a few micrometers. Various particle dynamics methods to simulate carbon nanostructures were applied in order to decrease the simulation time in comparison to ab initio approaches: molecular dynamics (Golovnev et al., 2008; Jin and Yuan, 2003; Reddy et al., 2006; Yao et al., 2001) and molecular mechanics (Korobeynikov et al., 2014). These methods suggest that atoms interact as material points through the empirical interaction potentials. In turn, these potentials are partly based on the quantum mechanical calculations. Such approaches reduce the problem to the solution of the ordinary differential equations at each time step. In addition, they require significantly less computational cost than ab initio methods.

At the same time it was shown (Berinskii and Krivtsov, 2010; Zhang et al., 2002) that a number of commonly used interaction potentials to simulate the graphene, graphite and diamond bonds (Allinger et al., 1989; Brenner et al., 2002; Tersoff, 1988) do not meet the experimentally determined elastic moduli. Furthermore, the empirical interaction potentials depending on the position of a number of particles include a large number of parameters with no clear physical meaning. At the same time they are inferior to the pairwise potentials of the Lennard-Jones or Morse type that depend only on the difference between the position vectors of the interacting particles. However, the classical pairwise potentials do not adequately describe the majority of covalent structures, which include carbon allotropes. Such structures are characterized by a low crystal packing density and oriented interatomic bonds. The use of a pairwise potential leads to the maximizing of a packing density that in turn causes the collapsing of a model. A possible

* Corresponding author.
E-mail address: iberinsk@gmail.com (I.E. Berinskii).

http://dx.doi.org/10.1016/j.ijsolstr.2016.06.014
0020-7683/

solution is to take the rotational degrees of freedom for the carbon atoms into account (Grekova and Zhilin, 2001; Ivanova et al., 2007; Vasiliev et al., 2010) and develop a generalized moment (torque) potentials (Berinskii et al., 2007; Kuzkin and Krivtsov, 2011; Kuzkin and Asonov, 2012; Tovstik and Tovstik, 2012) for simulations. In these works the atoms are assumed to be the solid bodies, not just the material points, and interaction between them is described both by the forces and the torques. It gives the interatomic bond additional lateral stiffness, providing the desired angle between the bonds in the lattice. Torque potentials combine the relative simplicity (they are, in fact, pairwise) and versatility. They independently determine the longitudinal, lateral, torsional and flexural bond rigidity. On the one hand it gives the freedom to choose the parameters of the simulation. On the other hand, if the longitudinal and lateral stiffness can be unambiguously determined from the experimentally measured elastic characteristics, the flexural and torsional bond stiffness depends on the couple-stress tensor components of the crystal lattice, for which to date there is no experimental data. On the macrolevel taking the rotational degrees of freedom into account allows to construct a generalised model of material (Eremeyev et al., 2012; Forest et al., 2000; Maugin and Metrikine, 2010).

The foregoing approaches can be attributed to the discrete methods, meaning that the crystal lattice is considered to be a set of interacting particles. However, there are some other approaches that are closer to the field of the classical mechanics. Such approaches are so–called structural or discrete–continuous methods (Cheng et al., 2009; Goldstein et al., 2008; Kalamkarov et al., 2006). The most straightforward example of the structural method is a covalent bond modeled by the solid deformable rod (Li and Chou, 2003; Tserpes and Papanikos, 2005). The distinction of these methods from the discrete ones consists in that the interatomic bonds are modeled as a deformable body or a construction. Besides the perception simplicity, these approaches have one more important advantage. They can be implemented in standard computing packages based on the finite–element, boundary–element, or finite difference methods. These methods can be considered as the bridges between the parameters of atomistic and continual models of the material. E.g. the classical elastic continual model has to be isotropic in case of graphene (Berinskii and Borodich, 2013a) and therefore has only two independent parameters.

The interatomic bond energy can be specified by a interatomic potential as a function of the distance between the nearest interacting atoms and the angles between the adjacent bonds in the lattice. The parameters of the potentials are chosen based on the elastic properties of the entire lattice. At the same time, the binding energy is equivalent to the energy of the rod deformation that depends on its length and its angular deflection. By comparing the energies one can determine the parameters required for the rod model. In particular, if the Euler–Bernoulli model of the rod is considered, then the parameters are Young's modulus of the bond and its diameter. More complex models can be used, e.g. the Timoshenko beam. However in this case an additional parameter appears namely the Poisson ratio of the rod. Its exact value cannot be determined (Berinskii et al., 2014). The circular section rod model imposes some limitations on the properties of carbon bond, but at the same time it allows to determine not only the longitudinal and transverse, but also the torsional and flexural stiffness using only two parameters. These parameters are necessary to determine the bending stiffness of a crystal lattice of the graphene sheet (Berinskii et al., 2014). Modelling of the graphene layer deformation with regard to the available experimental data shows that the ratio of the lateral bond stiffness C_2 between the carbon atoms to the longitudinal stiffness C_1 is approximately 1/2 (Ivanova et al., 2007). However, the rod bond model at the reasonable parameters

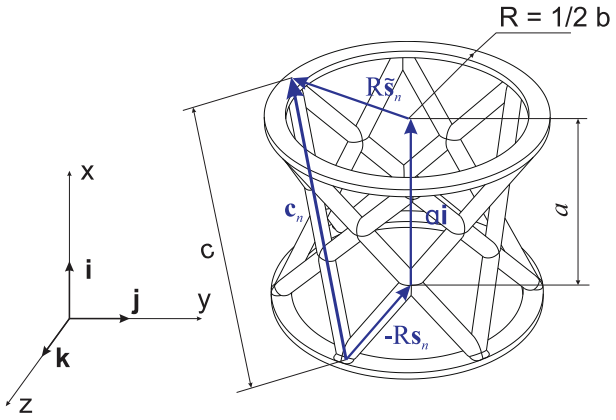

Fig. 1. 3D model of the carbon interatomic bond.

give a much lower value of the flexural rigidity. Thus, the value of 1/2 can only be achieved if the thickness of the rod is close to its length and the material of the rod should have the negative Poisson ratio (Berinskii and Borodich, 2013b). So, an important issue is to find a relatively simple mechanical model that allows for such a ratio of stiffness.

There are other conclusive structural models of the graphene and nanotubes, e.g. (Goldstein et al., 2008; Odegard et al., 2002). However, we have shown earlier (Berinskii and Borodich, 2013b) that they cannot meet the required stiffness ratio.

In this paper, the carbon bond model is built on the symmetry properties of the hyperboloid. These properties allow it to achieve a high ratio of the lateral and longitudinal stiffness, therefore the hyperboloid shapes are widely used in the engineering to create lightweight constructions consisting of straight beams that are known for being able to carry a large load while achieving a low use of raw materials. In particular, the first hyperboloid tower was built by Russian engineer V.G. Shukhov in Nizhny Novgorod (1896) (English, 2005). Being widely demanded in architecture and engineering, such models still haven't found a wide use in micro- and nanomechanics. It appears that the analogy drawn from the macro level will allow to describe correctly the properties of carbon materials at the micro level.

2. A hyperboloid carbon model: compression and tension stiffness

We model a carbon bond as a rigid structure, which is constructed as follows. Let us introduce the unit vectors of Cartesian basis **i, j, k**. Here and after the vector and tensor values are denoted by bold letters. Unit vector **i** determines a direction of the bond, unit vectors **j** and **k** determine a plane perpendicular to the bond. Next, consider a cylinder with an axis coinciding with the bond direction, and with the height equal to its length. Bases of the cylinder have a radius of $R = b/2$, where b is a bond width.

Then place a set of N truss elements with stiffness k along the generatrices of the cylinder so that they are evenly distributed over the cylinder surface. We then rotate one of the bases of the cylinder around its axis until it makes an angle γ. Then the trusses will rest on the one-sheet hyperboloid surface connecting the two cylinder bases (Figs. 1 and 2). Vectors $\mathbf{c}_n$ connecting the start and the end point of the truss members of hyperboloid may be represented as

$$\mathbf{c}_n \stackrel{\text{def}}{=} -R\mathbf{s}_n + a\mathbf{i} + R\tilde{\mathbf{s}}_n, \tag{1}$$

where

$$\mathbf{s}_n \stackrel{\text{def}}{=} \mathbf{P}\left(\frac{2n\pi}{N}\mathbf{i}\right)\cdot\mathbf{j}, \quad \tilde{\mathbf{s}}_n \stackrel{\text{def}}{=} \mathbf{P}(\gamma\mathbf{i})\cdot\mathbf{s}_n; \quad n = 1, 2, \ldots, N; \tag{2}$$

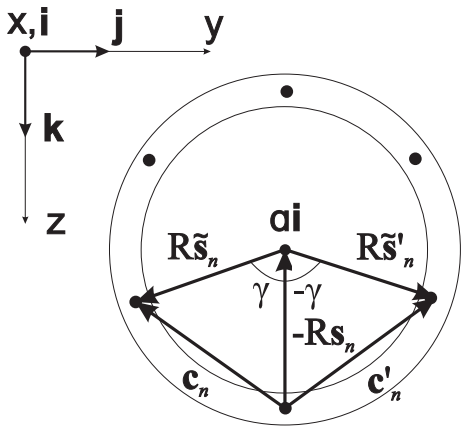

Fig. 2. Model of the carbon interatomic bond (top view).

The unit vectors $\mathbf{s}_n$ and $\tilde{\mathbf{s}}_n$ specify the attachment points of the trusses to the base of the cylinder. $\mathbf{P}(\gamma\mathbf{i})$ denotes the turn–tensor around unit vector i by angle γ (Grekova and Zhilin, 2001).

The resulting structure will have tension and shear stiffness, but will not have a torsion stiffness. To eliminate this shortcoming, we introduce the second set of N truss members of hyperboloid, twisted in the opposite direction (Fig. 2):

$$\mathbf{c}'_n \stackrel{\text{def}}{=} -R\mathbf{s}_n + a\mathbf{i} + R\tilde{\mathbf{s}}'_n, \quad \tilde{\mathbf{s}}'_n \stackrel{\text{def}}{=} \mathbf{P}(-\gamma\mathbf{i})\cdot\mathbf{s}_n. \tag{3}$$

If $\gamma = \pi/N$, then the set of trusses of the first and the second type form a side surface of the antiprism, which is a polyhedron with two N-gon end faces and $2N$ triangular lateral faces. The geometrical properties of the interatomic bond are considered in more details at Appendix B.

A stiffness tensor of the resulting structure has the form

$$\mathbf{C} = \frac{k}{c^2}\sum_n \left(\mathbf{c}_n\mathbf{c}_n + \mathbf{c}'_n\mathbf{c}'_n\right), \tag{4}$$

where c is the modulus of the corresponding vectors:

$$c = |\mathbf{c}_n| = |\mathbf{c}'_n| = \sqrt{R^2(\mathbf{s}_n - \tilde{\mathbf{s}}_n)^2 + a^2} = \sqrt{2R^2(1-\cos\gamma) + a^2}. \tag{5}$$

Let us calculate the sum

$$\sum_n \mathbf{c}_n\mathbf{c}_n = \sum_n \left(R^2(\mathbf{s}_n - \tilde{\mathbf{s}}_n)(\mathbf{s}_n - \tilde{\mathbf{s}}_n) + a^2\mathbf{i}\mathbf{i}\right). \tag{6}$$

Here we implement $\sum_n \mathbf{s}_k = \sum_n \tilde{\mathbf{s}}_k = 0$. By virtue of the symmetry, $N > 2$

$$\sum_n (\mathbf{s}_n - \tilde{\mathbf{s}}_n)(\mathbf{s}_n - \tilde{\mathbf{s}}_n) = \frac{N}{2}(\mathbf{s}_n - \tilde{\mathbf{s}}_n)^2\tilde{\mathbf{E}} = N(1-\cos\gamma)\tilde{\mathbf{E}}, \tag{7}$$

where $\tilde{\mathbf{E}} = \mathbf{j}\mathbf{j} + \mathbf{k}\mathbf{k}$ is a unit tensor in the plane perpendicular to the bond. Upon substituting these values in formula (4) for the stiffness tensor, one obtains:

$$\mathbf{C} = \frac{2Nk}{c^2}\left(R^2(1-\cos\gamma)\tilde{\mathbf{E}} + a^2\mathbf{i}\mathbf{i}\right). \tag{8}$$

Formula (8) gives the following expressions for the longitudinal and lateral stiffness

$$C_1 = 2Nk\frac{a^2}{c^2}, \quad C_2 = 2Nk\frac{R^2}{c^2}(1-\cos\gamma). \tag{9}$$

Consideration of torsion and bending of the hyperboloid bond (see Appendix C and Appendix D) gives the following formulae:

$$C_3 = 2Nk\frac{R^4}{c^2}\sin^2\gamma, \quad C_4 = \frac{R^2a^2kN}{2c^2}(1+\cos\gamma) \tag{10}$$

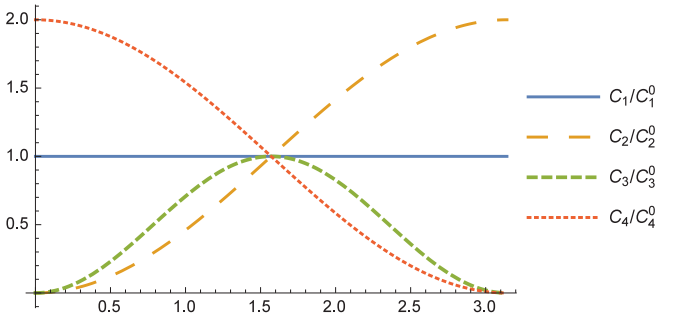

Fig. 3. Longitudinal, transversal, torsional and bending stiffness as the functions of angle γ.

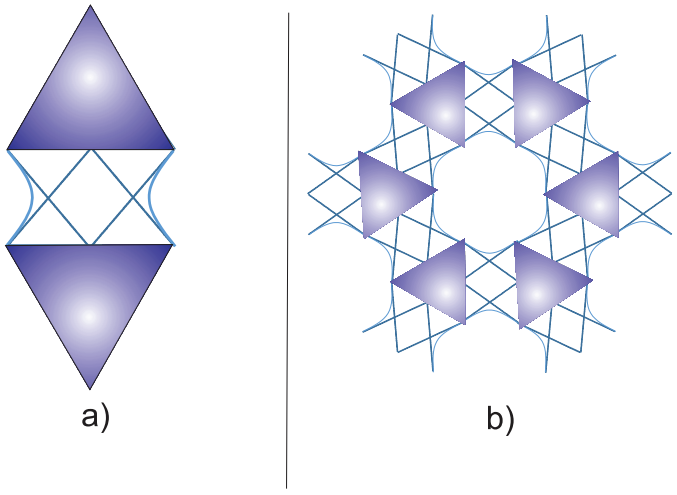

Fig. 4. (a) an interatomic bond between two atoms, (b) a typical hexagon of graphene crystal lattice.

where C_3 is a torsional and C_4 is a bending stiffness respectively. Let us represent every stiffness as

$$C_1 = C_1^0, \quad C_2 = C_2^0(1-\cos\gamma), \quad C_3 = C_4^0\sin^2\gamma, \quad C_4 = C_4^0(1+\cos\gamma) \tag{11}$$

where $C_1^0 - C_4^0$ are constant values which can be obtained form (10) and (11). Fig. 3 shows the dependencies of $C_1 - C_4$ on γ. One can see that at $\gamma = \pi/2$ all functions are far from zero. C_1, C_2 and C_4 have the mean values, at the same time C_3 has its maximum value. Hence, the case $\gamma = \pi/2$ is natural for practical applications.

Using the model of the interatomic bond proposed above and taking the symmetry of the crystal lattice into account it is possible to construct the model of given material. For instance, the model proposed for graphene is shown at Fig. 4. Ghaphene and carbon nanotubes have covalent sp2 bonds leading to the hexagonal symmetry of crystal lattice (Cooper et al., 2012; Pierson, 2012). The carbon atoms at Fig. 4 are represented as the triangles to take this symmetry into account. It does not mean that carbon atoms in such model have to be always simulated as the rigid triangles. However, sometimes this representation can be successfully used (Berinskii et al., 2007). In case of diamond one has sp3 hybridized carbon bond (Pierson, 2012), and the atoms can be represented as regular tetrahedrons (Fig. 5). Other carbons allotropes (Falcao and Wudl, 2007) also can be considered with hyperboloid model.

3. Ratios between the bond stiffness in different directions

As it was mentioned in introduction, the relation C_2/C_1 for carbon materials often exceeds 1/2. It will be shown later that some

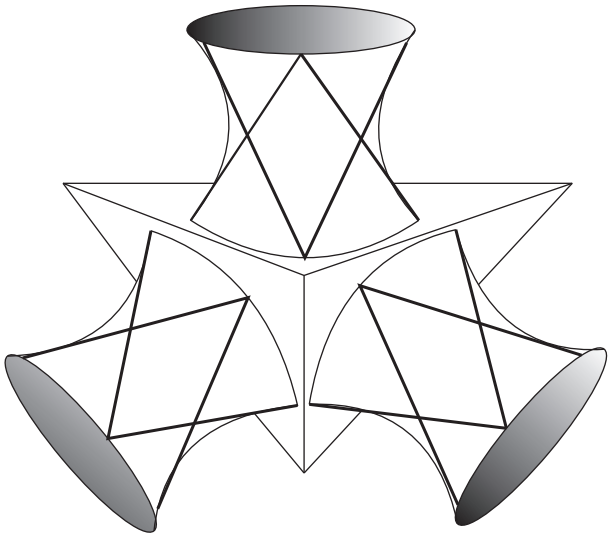

Fig. 5. Representation of sp3 hybridized carbon atom (diamond).

simple models can not satisfy this relation with reasonable parameters. Let us consider the relation mentioned above for hyperboloid model.

$$\frac{C_2}{C_1} = \frac{R^2}{a^2}(1-\cos\gamma) = \frac{b^2}{a^2}\,\frac{1-\cos\gamma}{4}, \tag{12}$$

where $b = 2R$ is the bond width. In the two-dimensional case the stiffness ratio is b^2/a^2. According to the formula (12), the maximum stiffness ratio is reached at $\gamma = \pi$. However, $\gamma = \pi$ case is degenerate because all the trusses intersect at a single point. Another case, $\gamma = \pi/2$, is more realistic, so we write:

$$\frac{C_2}{C_1} = \frac{R^2}{a^2} = \frac{1}{4}\,\frac{b^2}{a^2}. \tag{13}$$

For instance, the value for the stiffness ratio 1/2 is attained at

$$R = \frac{\sqrt{2}}{2}\,a \approx 0.7a, \quad b = \sqrt{2}\,a \approx 1.4a. \tag{14}$$

Hence, the thickness of hyperboloid can exceed it's length and it does not contradicts the physical sense unlike the rod models of the bond. Let us calculate then the corresponding value of c

$$c = \sqrt{a^2+b^2} = \sqrt{3}a \approx 1.7a. \tag{15}$$

Then we get the bond stiffness

$$C_1 = \frac{1}{3}C, \quad C_2 = \frac{1}{6}C; \quad C \stackrel{\text{def}}{=} 2Nk. \tag{16}$$

Where C is the total truss members' stiffness.

We next write down stiffness (9) in the form

$$C_1 = C\cos^2\alpha, \quad C_2 = C\sin^2\alpha\,\frac{1-\cos\gamma}{4} = \frac{1}{2}C\sin^2\alpha\,\sin^2\frac{\gamma}{2}. \tag{17}$$

Where $C = 2Nk$, $\alpha = \arctan\frac{b}{a}$. Then we get the stiffness ratio

$$\frac{C_2}{C_1} = \tan^2\alpha\,\frac{1-\cos\gamma}{4} = \frac{1}{2}\tan^2\alpha\,\sin^2\frac{\gamma}{2}. \tag{18}$$

Similarly, one can obtain for C_3 and C_4

$$C_3 = \frac{1}{4}CR^2\sin^2\alpha\sin^2\gamma, \quad C_4 = \frac{1}{4}R^2\left(\frac{a^2}{c^2}\right)C(1+\cos\gamma). \tag{19}$$

A corresponding stiffness ratio can be found as:

$$\frac{C_3}{C_4} = \tan^2\alpha\,\frac{\sin^2\gamma}{1+\cos\gamma}. \tag{20}$$

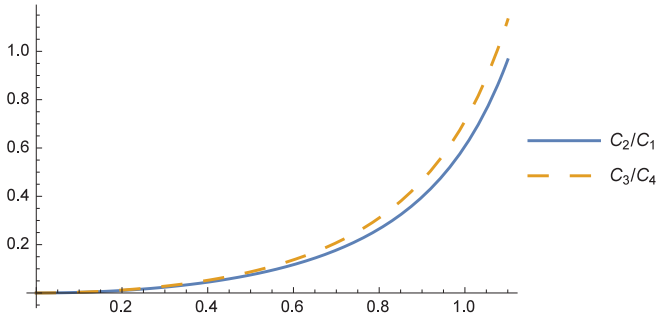

Fig. 6. Relations C_2/C_1 and C_3/C_4 as functions of angle $\alpha = \arctan\frac{b}{a}$ at $\gamma = \pi/2$.

Table 1
The stiffness ratio values.

γ	0	$\pi/2$	π
C_1/C	a^2/c^2	a^2/c^2	a^2/c^2
C_2/C	0	R^2/c^2	$2R^2/c^2$
C_3/C	0	R^4/c^2	0
C_4/C	$R^2a^2/(2c^2)$	$R^2a^2/(4c^2)$	0
C_2/C_1	0	R^2/c^2	$2R^2/c^2$
C_4/C_3	∞	$a^2/(4R^2)$	0

The functions of ratios on the angle α at $\gamma = \pi/2$ are shown at Fig. 6 Let us denote

$$\frac{C_2}{C_1} = \frac{\kappa^2}{2}, \tag{21}$$

where κ is undefined constant with order of unity. Then using (18) we obtain:

$$\tan\alpha\,\sin\frac{\gamma}{2} = \kappa. \tag{22}$$

It gives us the following representation for the trigonometric functions of argument α:

$$\tan\alpha = \frac{\kappa}{\sin\frac{\gamma}{2}}, \quad \sin\alpha = \frac{\kappa}{\sqrt{\kappa^2+\sin^2\frac{\gamma}{2}}}, \quad \cos\alpha = \frac{\sin\frac{\gamma}{2}}{\sqrt{\kappa^2+\sin^2\frac{\gamma}{2}}}, \tag{23}$$

and formulas (17) take the form

$$C_1 = \frac{\sin^2\frac{\gamma}{2}}{\kappa^2+\sin^2\frac{\gamma}{2}}C, \quad C_2 = \frac{1}{2}\,\frac{\kappa^2\sin^2\frac{\gamma}{2}}{\kappa^2+\sin^2\frac{\gamma}{2}}C. \tag{24}$$

In particular, if put $\kappa = 1$ and $\gamma = \pi/2$, one obtains values (16) for the stiffness. Similarly, we find the expressions for the torsional and flexural stiffness. In the general case using (C.8) and (23) we arrive at

$$C_3 = \frac{1}{4}\,\frac{\kappa^2\sin^2\gamma}{\kappa^2+\sin^2\frac{\gamma}{2}}CR^2 \tag{25}$$

For the bending stiffness formulas (D.18) and (23) result into

$$C_4 = \frac{1}{16}\,\frac{\kappa^2(1+\cos\gamma)}{\kappa^2+\sin^2\frac{\gamma}{2}}Ca^2 \tag{26}$$

The stiffness values for various γ are shown in Tables 1 and 2.

4. Comparison with the rod models

Let us compare the hyperboloid model and rod model of the carbon bonds. The longitudinal and transversal stiffness for the Euler–Bernoulli model (EBM) and the Timoshenko model (TM) are

Table 2
The stiffness ratio values, expressed in terms of $\alpha = \arctan\frac{b}{a}$.

γ	0	$\pi/2$	π
C_1/C	$\cos^2\alpha$	$\cos^2\alpha$	$\cos^2\alpha$
C_2/C	0	$\frac{1}{4}\sin^2\alpha$	$\frac{1}{2}\sin^2\alpha$
C_3/C	0	$\frac{R^2}{4}\sin^2\alpha$	0
C_4/C	$\frac{a^2}{8}\sin^2\alpha$	$\frac{a^2}{16}\sin^2\alpha$	0
C_2/C_1	0	$\frac{1}{4}\tan^2\alpha$	$\frac{1}{2}\tan^2\alpha$
C_4/C_3	∞	$\cot^2\alpha$	0

Table 3
Comparison of the models.

Model type	C_2/C_1	$(C_2/C_1)_{\max}$
EBM	$\frac{3}{4}\frac{b^2}{a^2}$	$\frac{3}{4}\frac{b^2}{a^2} \ll 1$
TM	$\frac{3}{4}\frac{\pi^2 b^2}{\pi^2 a^2 + 18(1+\nu)b^2}$	$\frac{\pi^2}{24} \approx 0.41$
HM	$\frac{1-\cos\gamma}{4}\frac{b^2}{a^2}$	$+\infty$

given (Berinskii et al., 2014). The longitudinal stiffness for both model is the same:

$$C_1^{EBM} = C_1^{TM} = \frac{EF}{a} \tag{27}$$

Here E is a rod Young modulus, F is a cross section and a is its length.

However, the transversal stiffness differ for two models. The Euler–Bernoulli model supposes the cross section is perpendicular to the bending line. In a Timoshenko model rotation between the cross section and the bending line is allowed. This makes the latter model more complicated and one need to take the additional parameters into account:

$$C_2^{EBM} = \frac{12EJ_2}{a^3}, \quad C_2^{TM} = \frac{12EJ_2kF}{kFa^3 + 24J_2(1+\nu)a} \tag{28}$$

Here ν is a Poisson's ratio, $k = \pi^2/12$ is a transverse shear parameter, J_2 is a section moment of inertia. Let us consider the rods with a circular section so that

$$F = \frac{\pi b^2}{4}, \quad J_2 = \frac{\pi b^2}{64} \tag{29}$$

Stiffness ratio values C_2/C_1 for the Euler–Bernoulli model (EBM), the Timoshenko model (TM), and the hyperboloid model (HM) proposed in this paper are presented in Table 3.

In addition, the table shows maximum possible stiffness ratio values C_2/C_1 attainable within the realistic range of parameters. Recall that ν is the dimensionless Poisson ratio of the rod material, which in principle can range from -1 to 0.5, but for the most of the real materials it varies from 0 to 0.5. The angle γ is a hyperboloid model parameter, ranging from 0 to π.

The Euler–Bernoulli model, as it is shown in the table, gives a result similar to the hyperboloid model, but with a higher stiffness (the value of the coefficient of b^2/a^2 in the BEM is higher than in HM). However, the Euler–Bernoulli model is derived under the assumption that the rod is thin, i.e. $b \ll a$. Therefore, it can properly describe only the small stiffness ratio values, while the experimental data provides the values close to 1/2. The hyperboloid model, by contrast, is defined for any b/a value, so it can provide any stiffness ratio from zero to infinity (it's impossible only in the degenerate case, if $\gamma = 0$).

Consider now the Timoshenko model. For the small values of b/a the results are actually the same as the results given by the Euler–Bernoulli model. On the contrary, if b/a tends to infinity, the model provides an expression, approaching the value $\frac{\pi^2}{24(1+\nu)}$ with no dependence on b/a. It takes the maximum value at $\nu = 0$ that gives $\frac{\pi^2}{24} \approx 0.41$, which is less than the required experimental value. Theoretically it is possible to achieve an arbitrarily large stiffness ratio when $\nu \to -1$, but the negative values of ν are not very natural. Additionally, even if b/a reaches a significant value, the use of the Timoshenko model instead of the Euler–Bernoulli model is fairly straightforward, but still controversial.

As a result, the aforementioned rod models allow to obtain the experimental stiffness ratio only if they are close to, or even out of the applicability range. The proposed hyperboloid model (HM) is free from these drawbacks, it allows to obtain the experimental stiffness ratio along with the reasonable parameter values. Thus, stiffness ratio 1/2 can be obtained for $\gamma = \pi/2$ and $b/a = \sqrt{2}$. Moreover, hyperboloid model allows to build a macroscopic model of a carbon bond and carbon nanostructures that can be used for the macroscopic simulation.

Table 4
Parameters of the bonds for graphene and diamond.

Material	C_1, N/m	C_2, N/m	a, nm	Source
Graphene	730	402	0.142	Ivanova et al. (2007)
Diamond	472	338	0.154	Krivtsov and Loboda (2012)

Table 5
Parameters of the bonds for graphene and diamond.

Material	b, nm	C, N/m	k, N/m (N=6)	k, N/m (N=12)
Graphene	0.203	2387	199	99
Diamond	0.260	1824	152	76

5. Parameters of hyperboloid bond for graphene and diamond

Let us now calculate the parameters of the proposed model for the real materials. The principal data are the values of transversal and longitudinal bond stiffness. These values were calculated previously and results are given in Table 4:

The data for graphene can be also used for carbon nanotubes and fullerens because these materials have the same type of carbon bond. Let us choose $\gamma = \pi/2$ due to the arguments considered in the previous sections. From (13) it follows:

$$b^2 = 4a^2\frac{C_2}{C_1}, \quad c^2 = a^2 + b^2 \tag{30}$$

Now the total trusses stiffness $C = 2Nk$ can be found from the first row of Table 1 as

$$C = C_1\left(1 + \frac{b^2}{a^2}\right) \tag{31}$$

The last question is how to choose number of trusses (N). From one point of view more truss members bring more accurancy to the model. On the other hand, big number of trusses make the model too complicated and uneffective for simulations. Determination of the optimal number of the trusses depends on the specific way of simulation and considered task. Here the truss stffness k is calculated for two cases that give the perfect symmetry to the bond and seem to be a reasonable choise: N = 6 and N = 12. The calculated parameters are given in Table 5.

The data from Tables 4 and 5 can be used for realization of specific model (e.g. finite element model). The trusses in such model can be sumulated as springs without mass or as the elastic rods.

6. Conclusion

The previous investigations have shown that model of carbon bond must reveal a ratio between the longitudinal and transverse

stiffness equal approximately 1/2. A significant disadvantage of the known structural models of carbon bonds is that they do not allow this ratio without loss of the physical meaning of the model. In this paper we proposed a hyperboloid shaped rod construction as a new mechanical model of the carbon bond. Rotation angle γ between the two bases of the construction is taken as a free model parameter. The influence of this parameter on the geometry of the carbon bond is estimated. The given work provides the stiffness ratio values computed for different γ. In particular, it is shown that the choices $\gamma = 0$ (corresponds to a cylindrical surface), and $\gamma = \pi$ (a conical surface) are the degenerate cases corresponding to the zero shear, torsional or bending stiffness. Selecting $\gamma = \pi/2$ allows to avoid the degenerate cases, and the structure in this case has the hyperboloid shape.

The following values are determined analytically: tension-and-compression (longitudinal) stiffness of the construction, shear (transverse) stiffness, the torsional stiffness about the symmetry axis, as well as the bending stiffness. The proposed model is compared with the Euler–Bernoulli and Timoshenko rod models that have been developed to simulate the carbon bonds earlier. It was shown that the hyperboloid model combined with the elastic properties of the rods allows to achieve the experimental ratio between the longitudinal and transverse carbon bond stiffness.

Acknowledgement

The authors would like to thank the reviewers for the deep analysis of this paper. The research was supported by the Ministry of Education and Science of Russian Federation within the project part of the government job in the field of scientific activity (task 9.2091.2014/ÏÚ) and by the Office of President of Russian Federation (Grant No. MK-4873.2014.1).

Appendix

Let us write the basic formulas describing the geometry and elastic properties of the three-dimensional hyperboloid bond.

Appendix A. Basic notation

a is a bond length; b is a bond width;

R is a bond radius, $R \stackrel{\text{def}}{=} \frac{1}{2} b$;

c is a truss length, $c \stackrel{\text{def}}{=} \sqrt{a^2 + b^2}$;

α is a bond width angle, $\alpha \stackrel{\text{def}}{=} \arctan \frac{b}{a}$;

γ is a bond torsion angle;

x is a coordinate along the bond; y is a coordinate across the bond;

k is truss stiffness; N is a number of the unidirectional truss members of hyperboloid;

C is a total trusses' stiffness, $C \stackrel{\text{def}}{=} 2Nk$;

C_1, C_2, C_3, C_4 are longitudinal, lateral,torsional and bending bond stiffness;

κ is a parameter of the covalency, $\kappa^2 \stackrel{\text{def}}{=} 2\frac{C_2}{C_1}$;

φ, Θ are the angles of hiperboloid torsion and bending respectively;

E, ν are the Young modulus and Poissone's ratio for EBM and TM;

F, J_2 are the section are and moment of inertia for EBM and TM;

M_T, M_B are the torque and the bending moment

Appendix B. Geometry of the hyperboloid bond model

Let us define the geometric characteristics of the three-dimensional bond. In the undeformed state the truss direction it

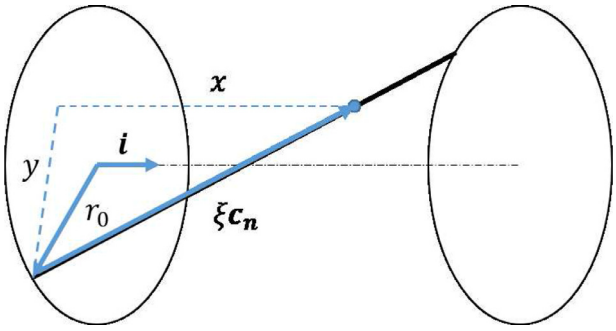

Fig. Appendix B.1. Geometry of hyperboloid bond.

defined by formula (1)

$$\mathbf{c}_n \stackrel{\text{def}}{=} -R\mathbf{s}_n + a\mathbf{i} + R\tilde{\mathbf{s}}_n, \tag{B.1}$$

where vector $\mathbf{c}_n$ connects the attachment points of the truss members of hyperboloid in the undeformed state. Let us introduce dimensionless variable ξ, taking the values from 0 to 1. Then the position of any point of the truss with respect to the bond center can be determined by a vector

$$\mathbf{r} \stackrel{\text{def}}{=} \mathbf{r}_0 + \mathbf{c}_n\xi, \quad \mathbf{r}_0 \stackrel{\text{def}}{=} -\frac{a}{2}\mathbf{i} + R\mathbf{s}_n. \tag{B.2}$$

Let us introduce projections

$$x \stackrel{\text{def}}{=} \mathbf{r}\cdot\mathbf{i}, \quad y \stackrel{\text{def}}{=} |\mathbf{r}\cdot(\mathbf{E} - \mathbf{ii})|. \tag{B.3}$$

For instance, x gives the vector projection on the direction of $\mathbf{i}$, and y is the projection length of x on a plane perpendicular to $\mathbf{i}$ (Fig. Appendix B.1). In other words, y expresses the distance from the point on the truss to the bond axis. Evaluating formulas (B.2) and (B.3) yields:

$$\begin{aligned} x &= a\xi - \frac{a}{2}, \quad y = R|(1-\xi)\mathbf{s}_n + \xi\tilde{\mathbf{s}}_n| \\ &= R\sqrt{(1-\xi)^2 + \xi^2 + 2(1-\xi)\xi\cos\gamma}. \end{aligned} \tag{B.4}$$

More convenient formulas can be obtained by introducing a new variable ζ:

$$\zeta = 2\xi - 1, \quad -1 \le \zeta \le 1. \tag{B.5}$$

Then formulas (B.5) take the form

$$x = \frac{a}{2}\zeta, \quad y = R\sqrt{\cos^2\frac{\gamma}{2} + \zeta^2\sin^2\frac{\gamma}{2}}. \tag{B.6}$$

Excluding ζ from these equations yields a hyperbola with respect to variables x and y.

$$\frac{y^2}{R^2} - \left(\frac{4}{a^2}\sin^2\frac{\gamma}{2}\right)x^2 = \cos^2\frac{\gamma}{2}. \tag{B.7}$$

Let us consider this equation for the three characteristic values of γ

$$\begin{aligned} &\gamma = 0: && y = R, \\ &\gamma = \frac{\pi}{2}: && 2\frac{y^2}{R^2} - 4\frac{x^2}{a^2} = 1, \\ &\gamma = \pi: && y = \pm 2\frac{R}{a}x. \end{aligned} \tag{B.8}$$

Thus, y is a constant when $\gamma = 0$, which corresponds to a cylindrical surface; if $\gamma = \pi$, then y varies linearly with x, which corresponds to a conical surface; if $\gamma = \frac{\pi}{2}$ then the function of y on x is a hyperbola.

Variables x and y range in values

$$-\frac{a}{2} \le x \le \frac{a}{2}, \quad y_{\min} \le y \le R, \tag{B.9}$$

where y reaches its minimum value at $x = 0$:

$$y_{\min} = R\cos\frac{\gamma}{2}. \tag{B.10}$$

In particular:

$$\gamma = \frac{\pi}{2} \quad \Rightarrow \quad y_{\min} = \frac{R}{\sqrt{2}} \approx 0.7R. \tag{B.11}$$

The derivative of y with respect to x if $x = a/2$ is equal to

$$\left.\frac{dy}{dx}\right|_{x=\frac{a}{2}} = 4\frac{R^2\sin^2\frac{\gamma}{2}}{a^2}\left.\frac{x}{y}\right|_{x=\frac{a}{2}} = 2\frac{R}{a}\sin^2\frac{\gamma}{2}. \tag{B.12}$$

In particular:

$$\gamma = \frac{\pi}{2} \quad \Rightarrow \quad \left.\frac{dy}{dx}\right|_{x=\frac{a}{2}} = \frac{R}{a}. \tag{B.13}$$

Appendix C. Torsional stiffness

Let us find the torque about axis x with unit vector $\mathbf{i}$ for the truss in the three-dimensional model. Imagine that the bottom side of the hyperboloid (1) was turned by an angle of φ about a unit vector $\mathbf{i}$. The corresponding torque of any separate truss element will be following:

$$\mathbf{M}_{\mathbf{n}T} = R\mathbf{s}_n \times \mathbf{F}_{\mathbf{n}T} \tag{C.1}$$

The force $\mathbf{F}_{\mathbf{n}T}$ for the given truss is determined by it's tensor of stiffness $\frac{k}{c^2}\mathbf{c}_n\mathbf{c}_n$ and displacement vector:

$$\mathbf{F}_{\mathbf{n}T} = \frac{k}{c^2}(\mathbf{c}_n\mathbf{c}_n)\cdot(-R\mathbf{s}_n\times\varphi\mathbf{i}) \tag{C.2}$$

Similarly, we have to take forces from other types of trusses into account:

$$\mathbf{F}'_{\mathbf{n}T} = \frac{k}{c^2}(\mathbf{c}'_n\mathbf{c}'_n)\cdot(-R\mathbf{s}_n\times\varphi\mathbf{i}) \tag{C.3}$$

The resulting torque will be given by sum

$$\mathbf{M}_T = \sum(\mathbf{M}_{\mathbf{n}T} + \mathbf{M}'_{\mathbf{n}T}) = -\sum_n R\mathbf{s}_n\times(\mathbf{F}_{\mathbf{n}T} + \mathbf{F}'_{\mathbf{n}T}) \tag{C.4}$$

Substitution of (C.2) and (C.3) to (C.4) gives:

$$\begin{aligned}\mathbf{M}_T &= -\sum_n R\mathbf{s}_n \times \frac{k}{c^2}\left(\mathbf{c}_n\mathbf{c}_n + \mathbf{c}'_n\mathbf{c}'_n\right)\cdot(R\mathbf{s}_n\times\varphi\mathbf{i}) \\ &= -\frac{kR^2\varphi}{c^2}\left(\sum_n \mathbf{s}_n\times\left(\mathbf{c}_n\mathbf{c}_n + \mathbf{c}'_n\mathbf{c}'_n\right)\times\mathbf{s}_n\right)\cdot\mathbf{i}\end{aligned} \tag{C.5}$$

Using expression (1) for $\mathbf{c}_n$ we get

$$\begin{aligned}&\mathbf{s}_n\times\mathbf{c}_n = a\mathbf{s}_n\times\mathbf{i} + R\mathbf{s}_n\times\tilde{\mathbf{s}}_n = a\mathbf{s}_n\times\mathbf{i} + R\mathbf{i}\sin\gamma, \\ &\mathbf{s}_n\times\mathbf{c}'_n = a\mathbf{s}_n\times\mathbf{i} + R\mathbf{s}_n\times\tilde{\mathbf{s}}'_n = a\mathbf{s}_n\times\mathbf{i} - R\mathbf{i}\sin\gamma, \\ &(\mathbf{c}_n\times\mathbf{s}_n)\cdot\mathbf{i} = -\left(\mathbf{c}'_n\times\mathbf{s}_n\right)\cdot\mathbf{i} = -R\sin\gamma;\end{aligned} \tag{C.6}$$

it follows

$$\begin{aligned}&\mathbf{M}_T = -\tfrac{kR^2\varphi}{c^2}\left(\textstyle\sum_n \mathbf{s}_n\times\left(\mathbf{c}_n\mathbf{c}_n + \mathbf{c}'_n\mathbf{c}'_n\right)\times\mathbf{s}_n\right)\cdot\mathbf{i} = \\ &= \tfrac{kR^2\varphi}{c^2}R\sin\gamma\textstyle\sum_n\Big((a\mathbf{s}_n\times\mathbf{i} + R\mathbf{i}\sin\gamma) - (a\mathbf{s}_n\times\mathbf{i} - R\mathbf{i}\sin\gamma)\Big) = \\ &= \tfrac{2NkR^4\varphi}{c^2}\sin^2\gamma\,\mathbf{i}.\end{aligned} \tag{C.7}$$

Thus, for torsional stiffness C_3 we arrive at

$$C_3 \stackrel{\text{def}}{=} \frac{|\mathbf{M}_T|}{\varphi} = 2Nk\frac{R^4}{c^2}\sin^2\gamma. \tag{C.8}$$

According to formula (C.8) if $\gamma = 0$ and $\gamma = \pi$ the torsional stiffness becomes zero and if $\gamma = \pi/2$, it achieves the maximum value. It is an additional argument to choose this value for γ. Comparing formulas (9) and (C.8) we find that the ratio of torsional and transverse stiffness is

$$\frac{C_3}{C_2} = \frac{R^2\sin^2\gamma}{1-\cos\gamma} = \frac{R^2\sin^2\gamma}{2\sin^2\frac{\gamma}{2}} = 2R^2\cos^2\frac{\gamma}{2}. \tag{C.9}$$

If $\gamma = \pi/2$, then the ratio of torsional and transverse stiffness is exactly equal to R^2.

Appendix D. Bending stiffness

Let us consider the bending stiffness of the hyperboloid bond. Consider the rotation of the bottom side of the hyperboloid (1) by an angle of Θ about a unit vector $\mathbf{k}$. The corresponding bending moment of separate truss element will be following:

$$\mathbf{M}_{\mathbf{n}B} = (-a\mathbf{i}/2 + R\mathbf{s}_n)\times\mathbf{F}_{\mathbf{n}B} \tag{D.1}$$

The force $\mathbf{F}_{\mathbf{n}B}$ for the given truss is determined by it's tensor of stiffness $\frac{k}{c^2}\mathbf{c}_n\mathbf{c}_n$ and displacement vector:

$$\mathbf{F}_{\mathbf{n}B} = \frac{k}{c^2}(\mathbf{c}_n\mathbf{c}_n)\cdot(-R\mathbf{s}_n\times\Theta\mathbf{k}) \tag{D.2}$$

Similarly, we have to take forces from other types of trusses into account:

$$\mathbf{F}'_{\mathbf{n}B} = \frac{k}{c^2}(\mathbf{c}'_n\mathbf{c}'_n)\cdot(-R\mathbf{s}_n\times\Theta\mathbf{k}) \tag{D.3}$$

The resulting moment will be given by sum

$$\mathbf{M}_B = \sum(\mathbf{M}_{\mathbf{n}B} + \mathbf{M}'_{\mathbf{n}B}) = -\sum_n(-a\mathbf{i}/2 + R\mathbf{s}_n)\times(\mathbf{F}_{\mathbf{n}B} + \mathbf{F}'_{\mathbf{n}B}) \tag{D.4}$$

Substitution of (D.2) and (D.3) to (D.4) gives the bending moment of the three-dimensional hyperboloid model arising from turning the end of the bond about $\mathbf{k} = \mathbf{s}_n\times\mathbf{i}$ by angle Θ:

$$\mathbf{M}_B = -\sum_n(-a\mathbf{i}/2 + R\mathbf{s}_n)\times\frac{k}{c^2}(\mathbf{c}_n\mathbf{c}_n + \mathbf{c}'_n\mathbf{c}'_n)\cdot(R\mathbf{s}_n\times\Theta\mathbf{k}) \tag{D.5}$$

Let us reformulate (D.5) as

$$\mathbf{M}_B = \frac{k}{c^2}R^2(\mathbf{C}_4^1 - (aR/2)\mathbf{C}_4^2)\cdot\Theta\mathbf{k} \tag{D.6}$$

where

$$\mathbf{C}_4^1 = \sum_n \mathbf{s}_n\times(\mathbf{c}_n\mathbf{c}_n + \mathbf{c}'_n\mathbf{c}'_n)\times\mathbf{s}_n \quad \mathbf{C}_4^2 = \sum_n \mathbf{i}\times(\mathbf{c}_n\mathbf{c}_n + \mathbf{c}'_n\mathbf{c}'_n)\times\mathbf{s}_n \tag{D.7}$$

Tensor $\mathbf{C}_4^1$ will be considered separately. Using the identities resulting from (1)–(3), one obtains:

$$\mathbf{s}_n\times\mathbf{c}_n = a\mathbf{s}_n\times\mathbf{i} + R\sin\gamma\,\mathbf{i} \quad \mathbf{s}_n\times\mathbf{c}'_n = a\mathbf{s}_n\times\mathbf{i} - R\sin\gamma\,\mathbf{i} \tag{D.8}$$

Then we have:

$$\mathbf{C}_4^1 = 2(a^2\mathbf{i}\times\sum_n \mathbf{s}_n\mathbf{s}_n\times\mathbf{i} - NR^2\sin^2\gamma\,\mathbf{i}\mathbf{i}) \tag{D.9}$$

It is easy to see that for the spherical tensor from (D.9), the following relation holds:

$$\sum_n \mathbf{s}_n\mathbf{s}_n = -(N/2)\tilde{\mathbf{E}} \tag{D.10}$$

Finally, we arrive at:

$$\mathbf{C}_4^1 = -N(a^2\tilde{\mathbf{E}} + 2R^2\sin^2\gamma\,\mathbf{i}\mathbf{i}) \tag{D.11}$$

Now, let us consider tensor $\mathbf{C}_4^2$. It is easy to see that

$$\mathbf{i}\times\mathbf{c}_n = R\mathbf{i}\times(\tilde{\mathbf{s}}_n - \mathbf{s}_n) \quad \mathbf{i}\times\mathbf{c}'_n = R\mathbf{i}\times(\tilde{\mathbf{s}}'_n - \mathbf{s}_n) \tag{D.12}$$

Taking into account (D.8) and (D.12), after transformations we get:

$$\mathbf{C}_4^2 = -Ra\mathbf{i}\times\sum_n(\mathbf{s}_n' + \tilde{\mathbf{s}}_n)\mathbf{s}_n\xi + 2aR\mathbf{i}\times\sum\mathbf{s}_n\mathbf{s}_n\mathbf{i} \tag{D.13}$$

Using (2) and (3) we wright

$$\mathbf{s}_n' + \tilde{\mathbf{s}}_n = (\mathbf{P}(\gamma\mathbf{i}) + \mathbf{P}\gamma\mathbf{i}))\cdot\mathbf{s}_n = 2\mathbf{i}\mathbf{i} + 2\tilde{\mathbf{E}}\cos\gamma \tag{D.14}$$

To obtain this relation we use the formula for a turn–tensor from Grekova and Zhilin (2001):

$$\mathbf{P}(\gamma\mathbf{i}) = \mathbf{i}\mathbf{i} + \cos\gamma(\tilde{\mathbf{E}} - \mathbf{i}\mathbf{i}) + \sin\gamma\mathbf{i}\times\tilde{\mathbf{E}} \tag{D.15}$$

Using (D.9), one can rearrange the second term in (D.13):

$$\mathbf{C}_4^2 = -aRN(1-\cos\gamma)\tilde{\mathbf{E}} \tag{D.16}$$

Introducing (D.11) and (D.16) into (D.6), one obtains the bending moment:

$$\mathbf{M}_B = -\frac{R^2a^2kN}{2c^2}(1+\cos\gamma)\Theta\mathbf{k} \tag{D.17}$$

whence we obtain the bending stiffness

$$C_4 = \frac{|\mathbf{M}_B|}{\Theta} = \frac{R^2a^2kN}{2c^2}(1+\cos\gamma) \tag{D.18}$$

N.b. that the maximum value of the bending stiffness is reached at $\gamma = 0$, but if $\gamma = \pi$ the bending stiffness becomes zero (the bond takes the shape of an hourglass in this case).

References

Allinger, N.L., Yuh, Y.H., Lii, J.H., 1989. Molecular mechanics: the MM3 force field for hydrocarbons. 1. J. Am. Chem. Soc. 111 (23), 8551–8566.

Berinskii, I., Borodich, F., 2013a. On the isotropic elastic properties of graphene crystal lattice. In: Surface Effects in Solid Mechanics. Springer, pp. 33–42.

Berinskii, I., Borodich, F.M., 2013b. Elastic in-plane properties of 2D linearized models of graphene. Mech. Mater. 62, 60–68.

Berinskii, I., Ivanova, E., Krivtsov, A., Morozov, N., 2007. Application of moment interaction to the construction of a stable model of graphite crystal lattice. Mech. Solids 42 (5), 663–671.

Berinskii, I., Krivtsov, A., 2010. On using many-particle interatomic potentials to compute elastic properties of graphene and diamond. Mech. Solids 45 (6), 815–834.

Berinskii, I., Krivtsov, A., Kudarova, A., 2014. Bending stiffness of a graphene sheet. Phys. Mesomech. 17 (4), 356–364.

Bichoutskaia, E., Heggie, M.I., Popov, A.M., Lozovik, Y.E., 2006. Interwall interaction and elastic properties of carbon nanotubes. Phys. Rev. B 73 (4), 045435.

Blakslee, O., Proctor, D., Seldin, E., Spence, G., Weng, T., 1970. Elastic constants of compression-annealed pyrolytic graphite. J. Appl. Phys. 41 (8), 3373–3382.

Bosak, A., Krisch, M., Mohr, M., Maultzsch, J., Thomsen, C., 2007. Elasticity of single-crystalline graphite: inelastic X-ray scattering study. Phys. Rev. B 75 (15), 153408.

Brenner, D.W., Shenderova, O.A., Harrison, J.A., Stuart, S.J., Ni, B., Sinnott, S.B., 2002. A second-generation reactive empirical bond order (REBO) potential energy expression for hydrocarbons. J. Phys. Condens. Matter 14 (4), 783.

Cheng, H.-C., Liu, Y.-L., Hsu, Y.-C., Chen, W.-H., 2009. Atomistic-continuum modeling for mechanical properties of single-walled carbon nanotubes. Int. J. Solids Struct. 46 (78), 1695–1704.

Cooper, D.R., D'Anjou, B., Ghattamaneni, N., Harack, B., Hilke, M., Horth, A., Majlis, N., Massicotte, M., Vandsburger, L., Whiteway, E., et al., 2012. Experimental review of graphene. ISRN Condens. Matter Phys. 2012.

English, E.C., 2005. Vladimir Shukhov and the invention of hyperboloid structures. In: Metropolis & Beyond: Proceedings of the 2005 Structures Congress and the 2005 Forensic Engineering Symposium.

Eremeyev, V.A., Lebedev, L.P., Altenbach, H., 2012. Foundations of micropolar mechanics. Springer Science & Business Media.

Falcao, E.H., Wudl, F., 2007. Carbon allotropes: beyond graphite and diamond. J. Chem. Technol. Biotechnol. 82 (6), 524–531.

Forest, S., Barbe, F., Cailletaud, G., 2000. Cosserat modelling of size effects in the mechanical behaviour of polycrystals and multi-phase materials. Int. J. Solids Struct. 37 (46), 7105–7126.

Geim, A.K., Novoselov, K.S., 2007. The rise of graphene. Nat. Mater. 6 (3), 183–191.

Goldstein, R., Osipenko, N., Chentsov, A., 2008. To determination of the strength of nanodimensional objects. Mech. Solids 43 (3), 453–469.

Golovnev, I., Golovneva, E., Fomin, V., 2008. Molecular dynamics calculation of thermodynamic properties of nanostructures. Phys. Mesomech. 11 (1), 19–24.

Grekova, E., Zhilin, P., 2001. Basic equations of Kelvin's medium and analogy with ferromagnets. J. Elas. Phys. Sci. Solids 64 (1), 29–70.

Iijima, S., et al., 1991. Helical microtubules of graphitic carbon. Nature 354 (6348), 56–58.

Ivanova, E., Krivtsov, A., Morozov, N., 2007. Derivation of macroscopic relations of the elasticity of complex crystal lattices taking into account the moment interactions at the microlevel. J. Appl. Math. Mech. 71 (4), 543–561.

Jin, Y., Yuan, F., 2003. Simulation of elastic properties of single-walled carbon nanotubes. Compos. Sci. Technol. 63 (11), 1507–1515.

Kalamkarov, A., Georgiades, A., Rokkam, S., Veedu, V., Ghasemi-Nejhad, M., 2006. Analytical and numerical techniques to predict carbon nanotubes properties. Int. J. Solids Struct. 43 (22), 6832–6854.

Korobeynikov, S., Alyokhin, V., Annin, B., Babichev, A., 2014. Quasi-static buckling simulation of single-layer graphene sheets by the molecular mechanics method. Math. Mech. Solids. 1081286514554353

Krivtsov, A.M., Loboda, O., 2012. Description of elastic properties of diamond-and sphalerite-structured diatomic crystals with the use of moment interaction. Phys. Mesomech. 15 (3–4), 238–244.

Kroto, H.W., Heath, J.R., O'Brien, S.C., Curl, R.F., Smalley, R.E., et al., 1985. C 60: Buckminsterfullerene. Nature 318 (6042), 162–163.

Kudin, K.N., Scuseria, G.E., Yakobson, B.I., 2001. C_2F, BN, and C nanoshell elasticity from ab initio computations. Phys. Rev. B 64 (23), 235406.

Kuzkin, V., Krivtsov, A., 2011. Description for mechanical properties of graphene using particles with rotational degrees of freedom. In: Doklady Physics, Vol. 56. Springer, pp. 527–530.

Kuzkin, V.A., Asonov, I.E., 2012. Vector-based model of elastic bonds for simulation of granular solids. Phys. Rev. E 86 (5), 051301.

Li, C., Chou, T.-W., 2003. A structural mechanics approach for the analysis of carbon nanotubes. Int. J. Solids Struct. 40 (10), 2487–2499.

Maugin, G.A., Metrikine, A.V., 2010. Mechanics of generalized continua. Adv. Mech. Math. 21.

McSkimin, H., Andreatch Jr, P., 1972. Elastic moduli of diamond as a function of pressure and temperature. J. Appl. Phys. 43 (7), 2944–2948.

McSkimin, H., Bond, W., 1957. Elastic moduli of diamond. Physical Review 105 (1), 116.

Odegard, G.M., Gates, T.S., Nicholson, L.M., Wise, K.E., 2002. Equivalent-continuum modeling of nano-structured materials. Compos. Sci. Technol. 62 (14), 1869–1880.

Pierson, H.O., 2012. Handbook of Carbon, Graphite, Diamonds and Fullerenes: Processing, Properties and Applications. William Andrew.

Reddy, C., Rajendran, S., Liew, K., 2006. Equilibrium configuration and continuum elastic properties of finite sized graphene. Nanotechnology 17 (3), 864.

Tersoff, J., 1988. Empirical interatomic potential for carbon, with applications to amorphous carbon. Phys. Rev. Lett. 61 (25), 2879.

Tovstik, P., Tovstik, T., 2012. Static and dynamic analysis of two-dimensional graphite lattices. Mech. Solids 47 (5), 517–524.

Tserpes, K., Papanikos, P., 2005. Finite element modeling of single-walled carbon nanotubes. Compos. Part B Eng. 36 (5), 468–477.

Vasiliev, A., Dmitriev, S., Miroshnichenko, A., 2010. Multi-field approach in mechanics of structural solids. Int. J. Solids Struct. 47 (3), 510–525.

Yanovsky, Y.G., Nikitina, E., Karnet, Y.N., Nikitin, S., 2009. Quantum mechanics study of the mechanism of deformation and fracture of graphene. Phys. Mesomech. 12 (5), 254–262.

Yao, Z., Zhu, C.-C., Cheng, M., Liu, J., 2001. Mechanical properties of carbon nanotube by molecular dynamics simulation. Comput. Mater. Sci. 22 (34), 180–184.

Zhang, P., Huang, Y., Geubelle, P., Klein, P., Hwang, K., 2002. The elastic modulus of single-wall carbon nanotubes: a continuum analysis incorporating interatomic potentials. Int. J. Solids Struct. 39 (13), 3893–3906.

Zhou, G., Duan, W., Gu, B., 2001. First-principles study on morphology and mechanical properties of single-walled carbon nanotube. Chem. Phys. Lett. 333 (5), 344–349.